Size effects in polycrystalline thin films analyzed by discrete dislocation plasticity

Nicola, L; Van der Giessen, E; Needleman, A

Published in:
Thin Solid Films

DOI:
10.1016/j.tsf.2004.12.012

Publication date:
2005

Available online at www.sciencedirect.com

SCIENCE DIRECT®

Thin Solid Films 479 (2005) 329–338

thin solid films

www.elsevier.com/locate/tsf

Size effects in polycrystalline thin films analyzed by discrete dislocation plasticity

Lucia Nicola[a], Erik Van der Giessen[a,*], Alan Needleman[b]

[a]*The Netherlands Institute for Metals Research/Dept. of Applied Physics, University of Groningen, Nyenborgh 4, 9747 AG Groningen, The Netherlands*

[b]*Division of Engineering, Brown University, Providence, RI 02912, USA*

Received 22 March 2004; accepted in revised form 3 December 2004

Available online 20 January 2005

Abstract

Stress development and relaxation in polycrystalline thin films perfectly bonded to a stiff substrate is analyzed numerically. The calculations are carried out within a two-dimensional plane strain framework. The film–substrate system is subject to a prescribed temperature decrease, with the coefficient of thermal expansion of the metal film larger than that of the substrate. Plastic deformation arises solely from the glide of edge dislocations. The dislocations nucleate from pre-existing Frank–Read sources, with the grain boundaries and film–substrate interface acting solely as impenetrable barriers to dislocation glide. At each stage of loading, a boundary value problem is solved to enforce the boundary conditions and the stress field and the dislocation structure are obtained. The results of the simulations show both film-thickness and grain size dependent strengthening of polycrystalline films. Limited plasticity occurs in films with a sufficiently small grain-size, mainly due to a reduced nucleation rate in the constrained grain geometry.

PACS: 61.72.Lk; 62.20.Fe; 68.60.Bs

Keywords: Stress; Grain boundary; Interface; Dislocation dynamics

1. Introduction

The drive to produce smaller electronic devices has motivated research on the mechanical behavior of components at the micro- and nano-scale. In contrast to classical plasticity, which predicts a size independent response, the flow strength in small structures (with at least one dimension of the order of micrometers) is typically higher than in the corresponding bulk material [1–3]. In order to understand this size dependence, much attention has been focused on the role of material length scales and their effect on flow strength.

A representative situation is a thin metal film on a stiff substrate which leads to tensile loading of the film on cooling from processing temperatures, due to the mismatch in thermal expansion coefficient between the film and the substrate. As cooling proceeds from an almost stress-free state at a relatively high temperature, the deformation is initially elastic, but plastic deformation eventually occurs. With decreasing film thickness, the amount of plastic deformation also decreases [4,5]. Although there is only one relevant geometric length, the film thickness, films typically are polycrystals so that the grain size provides another relevant length scale. With the usual deposition techniques, the film thickness and grain size cannot be varied independently; the grains have a columnar structure with an average size approximately equal to the film thickness [6]. Therefore, it is generally difficult experimentally to ascertain the relative roles of grain size and film thickness. Experiments to measure stress evolution at constant grain size have been carried out by Venkatraman and Bravman [4] and more recently by Xiang et al. [7] on free-standing thin films. The simulations presented in this paper are motivated by these experiments.

* Corresponding author. Tel.: +31 50 363 8047; fax: +31 50 363 4886.
E-mail address: E.van.der.Giessen@rug.nl (E. Van der Giessen).

0040-6090/$ - see front matter © 2004 Elsevier B.V. All rights reserved.
doi:10.1016/j.tsf.2004.12.012

The analyses are carried out within a two-dimensional discrete dislocation plasticity framework [8] with the substrate and the grain boundaries regarded as impenetrable obstacles to glide. The elastic interactions among multiple dislocations, dislocation nucleation, glide and annihilation are accounted for. Other possible deformation and damage mechanisms such as dislocation climb, grain boundary diffusion and sliding, void growth, phase transformation, delamination and cracking are neglected. The simplicity of the model allows isolation of the effect of geometrical constraint arising from the substrate and the grain boundaries on dislocation activity in thin films. In addition, there is a wide temperature range for which plastic deformation is dominated by dislocation glide [9].

2. Problem formulation and method of analysis

The polycrystalline film is modeled as an infinitely long planar array of rectangular grains perfectly bonded to a semi-infinite elastic substrate (Fig. 1). Plane strain conditions are assumed and elastic anisotropy of the grains and of the substrate is neglected. Plasticity in the film originates from the motion of the straight edge part of threading dislocations in the x_1–x_2 plane. The film is periodic in x_1 direction with a cell of width w, which is taken to contain eight grains. Each grain, of height h and width d, contains three sets of slip planes on which edge dislocations, with Burgers vector $\boldsymbol{b}$, can nucleate and glide. The angle between the three slip planes in each grain is 60°, and the orientation of grain γ is identified by the angle ϕ^{γ} with the film–substrate interface x_2=0, see Fig. 1. The orientation of each grain is chosen randomly, even though such an extreme situation may be difficult to obtain in practice, where films are often textured and grains would be separated by low angle grain boundaries. The grain boundaries as well as the film–substrate interface are taken to be flat and impenetrable to dislocations. In real films, penetrability of the interface and the grain boundaries depends on the materials involved and on the deposition process. The smaller the misorientation between the grains, the larger their penetrability to dislocations; while softer substrates will be more penetrable than stiff ones. We avoid this additional complexity to highlight the role of confinement and to circumvent the necessity of introducing additional parameters.

The film and substrate are taken to have the same elastic constants. Accounting for different elastic properties requires computation of polarization stresses, which considerably increases the computing time. We have investigated the effect of elastic mismatch for single crystal aluminum films on silicon substrates and found that even with this elastic mismatch the polarization stresses have a negligible influence on the overall mechanical response [10]. The coefficients of thermal expansion α_f and α_s, for the film and substrate respectively, are taken to differ, with $\alpha_f > \alpha_s$: cooling of the film–substrate system leads to a tensile stress in the film.

As long as the response remains elastic, the boundary value problem for the unit cell in Fig. 1 is governed by the equilibrium conditions for the stress σ_{ij}, the relation between strain ε_{ij} and displacement u_i, and the thermo-elastic constitutive law,

$$\varepsilon_{ij} = \frac{1+\nu}{E}\left(\sigma_{ij} - \frac{\nu}{1+\nu}\delta_{ij}\sigma_{kk}\right) + (\alpha_f - \alpha_s)(T - T_0)\delta_{ij} \tag{1}$$

in which T is the temperature, T_0 is the temperature in the initial stress-free state, E is Young's modulus and ν is Poisson's ratio. Plastic deformation when it occurs is described by the motion of discrete dislocations represented as line singularities in the thermo-elastic film material. When dislocations are present, the set of governing equations is extended with a set of constitutive rules for dislocation motion.

Since we focus on stress development in the thin film, the unconstrained contraction that the film–substrate system undergoes with decreasing the temperature is neglected; this strain can be added to the strain fields calculated here to give the total strain (as discussed for the single crystal film analysis in [10]). The bottom of the substrate is fully clamped, i.e. u_1=u_2=0 there. In the finite element calcu-

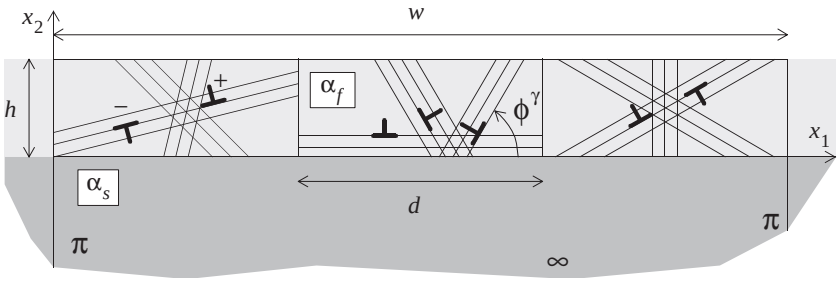

Fig. 1. Model of the polycrystalline film on a semi-infinite elastic substrate. Only three grains are shown in the schematic, while the simulations use eight grains per unit cell.

lations, the substrate is taken to be 100 times larger than the thickest film analyzed, which was large enough to mimic a semi-infinite substrate. Periodic boundary conditions are imposed on the unit cell,

$$u_i(0,x_2) = u_i(w,x_2), \tag{2}$$

while traction-free conditions characterize the film free-surface,

$$\sigma_{12}(x_1,h) = \sigma_{22}(x_1,h) = 0. \tag{3}$$

Because the elastic properties and thermal expansion coefficient are taken to be identical in each grain, the only non-vanishing stress component in the film, prior to dislocation nucleation, is $\sigma_{11}=\sigma_n$ which is given by:

$$\sigma_n = -\frac{(\alpha_f - \alpha_s)E(T-T_0)}{(1-\nu)}. \tag{4}$$

Once dislocations nucleate, the stress in the film is computed using superposition [8]: the singular $\tilde{\sigma}_{ij}^{(I)}$ fields (I=1,. . .,N) associated with the N dislocations in the unit cell and their replicas in the film are calculated analytically from the isotropic linear elastic, infinite medium fields. The complete solution is obtained by adding an image field $\hat{\sigma}_{ij}$ that ensures that the boundary conditions (2) and (3) on the unit cell are satisfied. Thus, the stress at each point is given by:

$$\sigma_{ij} = \hat{\sigma}_{ij} + \sum_{I=1}^{N} \tilde{\sigma}_{ij}^{(I)}.$$

The image fields are obtained by solving a linear elastic boundary value problem for the unit cell with boundary conditions changing as the dislocation structure evolves. The loading is imposed by a prescribed temperature T that decreases linearly with time.

3. Dislocation dynamics

At the beginning of the calculation the film is stress-free and dislocation-free. Dislocation sources are randomly distributed on the slip planes in the film, with a density $\rho_{nuc}=60/\mu m^2$. These point sources mimic Frank–Read sources inside the film and do not evolve during the simulation. Dislocation nucleation from grain boundaries or from the interface with the substrate is not incorporated in the present study. Thus, our calculations pertain to situations where the grain size and the film thickness are large enough for a significant density of entangled dislocations to be present and serve as Frank–Read sources, as seen for instance in 0.5 μm thin Cu films on Si in [11]. Each source is randomly assigned a nucleation strength τ_{nuc} from a Gaussian distribution with average 25 MPa and standard deviation 5 MPa. As the temperature of the film–substrate system decreases, an increasing homogeneous tensile stress develops in the film until dislocation nucleation occurs at the weakest Frank–Read source when the Peach–Koehler force at this source exceeds the nucleation strength $\tau_{nuc}b$ during the nucleation time τ_{nuc}=10 ns. The Frank–Read source generates a dislocation dipole with its sign being determined by the sign of the resolved shear stress. The distance between the two dislocations, L_{nuc}, is taken such that the attractive stress between them is equilibrated by a shear stress of magnitude τ_{nuc} at nucleation:

$$L_{nuc} = \frac{\mu}{2\pi(1-\nu)}\frac{b}{\tau_{nuc}}. \tag{5}$$

After nucleation, the dislocations glide apart, driven by the Peach–Koehler force acting on them. The Peach–Koehler force on dislocation I is calculated as:

$$f^{(I)} = n_i^{(I)}\left(\hat{\sigma}_{ij} + \sum_{J\neq I}\sigma_{ij}^{(J)}\right)b_j^{(I)}. \tag{6}$$

Dislocation glide is taken to be drag controlled, with zero Peierls stress, so that the velocity of dislocation I is computed directly from the Peach–Koehler force as $v^{(I)}=f^{(I)}/B$, with B being the drag coefficient, taken to have the value $B=10^{-4}$ Pa s.

As loading proceeds, other dislocation sources are activated. Dislocation nucleation at the Frank–Read sources and dislocation glide depend on both the applied thermal loading and the stress fields of the other dislocations. When two dislocations of opposite signs come closer to each other than the specified annihilation distance of $6b$, they are removed from the simulation.

4. Results

Simulations have been performed for polycrystalline films of thickness h=0.25, 0.5 and 1 μm for a grain size of d=0.25, 0.5 and 1 μm. The width of the unit cell is taken to scale with the grain size d and each cell consists of eight grains. Calculations were carried out for five realizations of each polycrystal. Each realization is characterized by the set of grain orientations ϕ^{γ} and the distribution of source locations and strengths. The temperature is decreased linearly with time from T_0=600 to 400 K at a cooling rate of $\dot{T}=40\times10^6$ K/s (to limit the computing time). Representative values for silicon and aluminum are taken for the linear thermal expansion coefficients of the substrate and film, respectively: $\alpha_s=4.2\times10^{-6}$/K and $\alpha_f=23.2\times10^{-6}$/K. The Burgers vector has a value representative of copper, b=0.25 nm.

The value of σ_{11}, the normal stress parallel to the interface, averaged over the film and then averaged over all realizations of each polycrystal is denoted by $\langle\sigma_{11}\rangle_f$. Curves of $\langle\sigma_{11}\rangle_f$ versus temperature T are shown in Fig. 2, where the same line thickness is used for films with

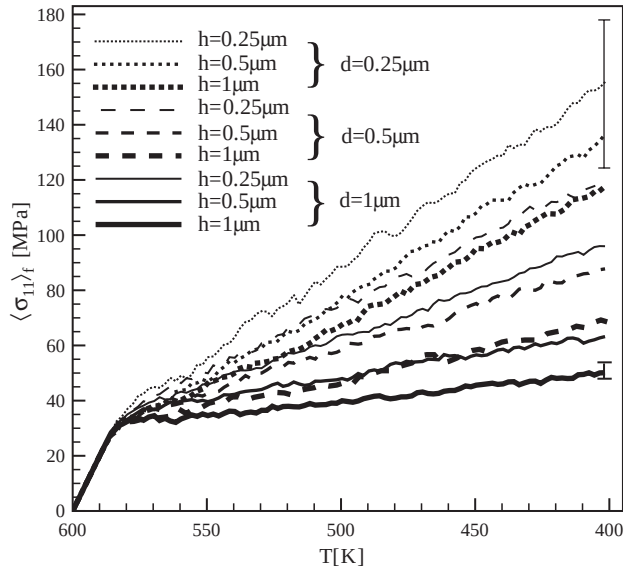

Fig. 2. Average stress in the film, $\langle\sigma_{11}\rangle_f$, versus temperature T for films of various thickness and grain size. Each curve is an average over five realizations with the values of film thickness h and grain size d but with different grain orientations and source distributions. The vertical bars indicate the range of stress values at T=400 K for the two extreme cases: for h=d=0.25 μm the spread is maximum and for h=d=1 μm the spread is minimum.

the same thickness h, but with different grain sizes. For a fixed film thickness, the smaller the grain size, the higher the hardening rate.

At the beginning of the cooling process $\langle\sigma_{11}\rangle_f$ increases linearly until, after approximately $T-T_0=-15$ K, plastic deformation starts at $\approx\langle\sigma_{11}\rangle_f$=38 MPa. This value depends on the choice of the nucleation strength τ_{nuc}. Subsequent hardening in the films depends on both the film thickness h and the grain size d. For each grain size, the hardening rate increases with decreasing film thickness and for a given film thickness, the hardening rate increases with decreasing grain size. Since these two effects reinforce each other, the small grain-thin film, h=d=0.25 μm, reaches the highest value $\langle\sigma_{11}\rangle_f$=155 MPa; the film with h=d=1 μm has the lowest value, $\langle\sigma_{11}\rangle_f$=50 MPa.

For the two extreme cases, h=d=0.25 μm and h=d=1 μm, the vertical lines in Fig. 2 show the spread in the stress level at 400 K for the five realizations. The spread is large, $\simeq$ 50 MPa, for the film with h=d=0.25 μm and only $\simeq$ 10 MPa for the film with h=d=1 μm. The larger the grain size d and the film thickness h, the less the spread among the various realizations. This is a statistical effect since the source density is constant (ρ_{nuc}=60 sources/μm^2) for all films, while the size of the unit cell scales with grain size and film thickness.

For each film a characteristic realization is chosen (i.e. the realization for which the stress–temperature curve is closest to the average) to show the stress distribution and the dislocation structure at 400 K in Figs. 3–5. In these figures the film region is shown together with a small part of the substrate near its interface with the film; the stress in the substrate is very low on average because of its large size. The stress is normalized by the elastic stress σ_n (Eq. (4)) that would develop in the absence of dislocations. Grain boundaries are indicated by vertical lines, positive dislocations by a +, and negative dislocations by a − (see Fig. 1). Common to all films is that, due to dislocation glide, the average stress is lower than the elastic stress σ_n (consistent with Fig. 2). Moreover, and in agreement with experimental findings by Phillips et al. [12], there is a considerable difference in plastic relaxation between grains as well as inside each grain.

In each case, a high-stress region is found at the interface between the film and the substrate. The dislocations that are in the films in Figs. 3–5 are not all the dislocations that have been nucleated during the deformation history: many dislocations have left the film through the free surface. For each nucleated dipole, one dislocation glides toward the film–substrate interface and the other toward the free surface. If both dislocations do not encounter an obstacle along their path, one stops against the impenetrable interface, while the other exits the film, leaving a displacement step in the free surface. However, in many cases, dislocations do find obstacles, which could be a dislocation pile-up on the same slip plane or dislocations on crossing slip planes, or a grain boundary, before reaching the free surface or the interface with the substrate. The total dislocation density in the film does not provide a direct indication of the stress relaxation. Stress relaxation is a consequence of dislocation glide, while a high density of dislocations can also occur when dislocations have been stopped by an obstacle before much

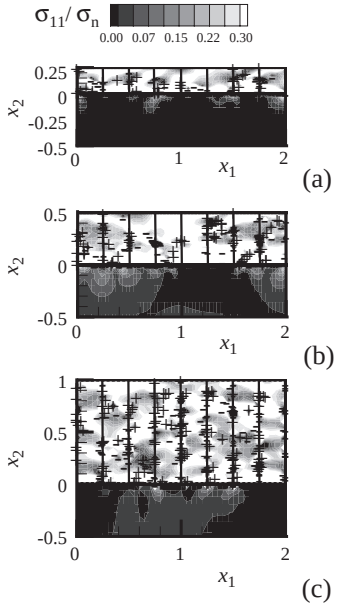

Fig. 3. Dislocation distribution and contours of σ_{11} at 400 K for films with grain size d=0.25 μm and various values of film thickness: (a) h=0.25 μm; (b) h=0.5 μm; and (c) h=1 μm. The + and − symbols denote positive and negative dislocations according to the sign convention in Fig. 1, and all dimensions are in μm.

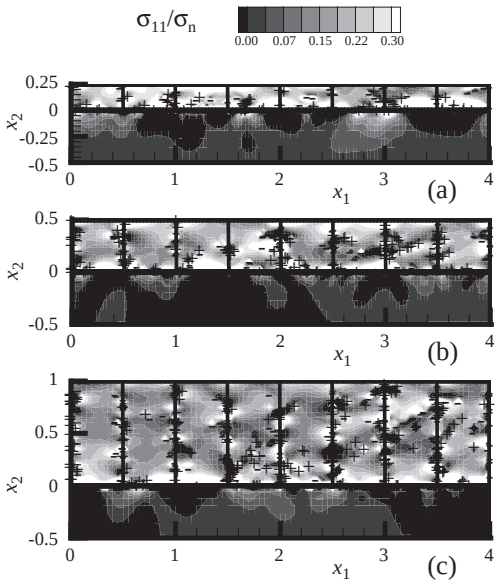

Fig. 4. Dislocation distribution and contours of σ_{11} at 400 K for films with grain size d=0.5 μm and various values of film thickness (a) h=0.25 μm; (b) h=0.5 μm; and (c) h=1 μm. The + and − symbols denote positive and negative dislocations according to the sign convention in Fig. 1, and all dimensions are in μm.

glide has occurred. What is more indicative of the stress relaxation is the number of dislocations that have arrived at the interface with the substrate. The glide of these dislocations has contributed to stress relaxation in the film. At the same time, however, the dislocations that pile-up at the film–substrate interface also attribute to the high stress region there. Comparison of the dislocation structure obtained at T=400 K in films of various thickness (Figs. 3–5) shows that long pile-ups form only in thicker films. This is more evident in the films with large grains. It is important to note that high stresses near the interface are also found in the absence of dislocation pile-ups, and are attributed to long-range effects of pile-ups against grain boundaries.

4.1. Thickness-dependent response

As seen in Fig. 2, for a given grain size the films exhibit a thickness-dependent response. In order to understand the origin of the thickness dependence, it is useful to examine the stress state in the films at the final temperature, 400 K. For various values of x_2 (where x_2 is the coordinate perpendicular to the interface, Fig. 1), the average value of σ_{11} along x_1 is calculated over the cell. This cell-average value is then averaged over all realizations for a given polycrystal (i.e. given values of h and d) and is denoted by $\langle\sigma_{11}\rangle$ (the average of this over x_2 is equal to the film average $\langle\sigma_{11}\rangle_f$ plotted in Fig. 2).

Fig. 6 shows curves of $\langle\sigma_{11}\rangle$ versus x_2. Each plot in Fig. 6 pertains to a fixed grain size. Fig. 6(a), for the films with smallest grain size, indicates that three regions can be identified in the films: (i) a region close to the free surface; (ii) a region close to the interface; and (iii) a central region. Regions (i) and (ii) are characterized by a high stress gradient and by a higher than average stress level. Region (iii) is characterized by an almost uniform value of $\langle\sigma_{11}\rangle$, which is lower than the average film stress. While the thickness of regions (i) and (ii) is approximately independent of the film thickness, the extent of region (iii) decreases with decreasing film thickness. What causes the thickness effect is that the size and average stress in the two boundary layers do not scale with the film thickness. Subsequently, region (i) will be referred to as the interface boundary layer,

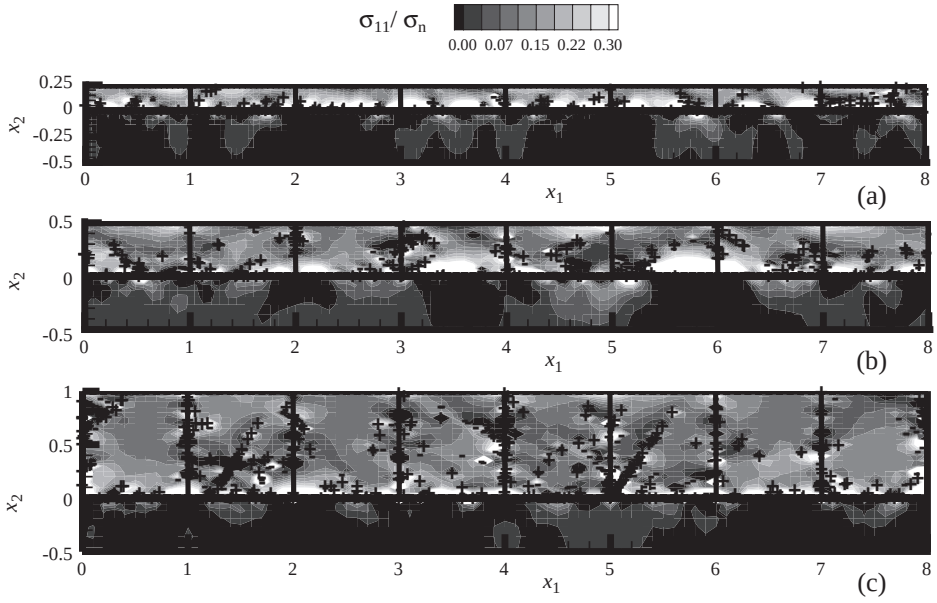

Fig. 5. Dislocation distribution and σ_{11} at T=400 K for films with grain size d=1 μm and various film thicknesses: (a) h=0.25 μm, (b) h=0.5 μm; and (c) h=1 μm. The + and − symbols denote positive and negative dislocations according to the sign convention in Fig. 1, and all dimensions are in μm.

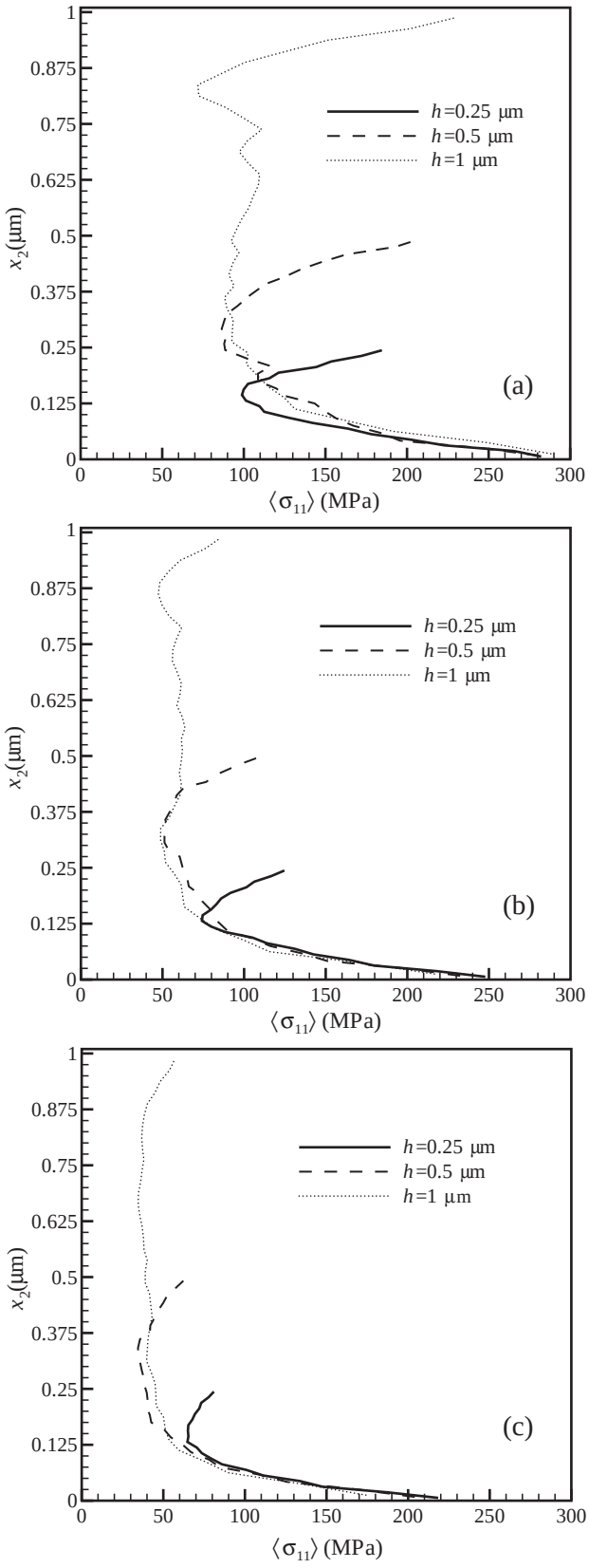

Fig. 6. Variation of average stress, $\langle\sigma_{11}\rangle$, across the film thickness for films of varying thickness and grain size: (a) d=0.25 μm, corresponding to Fig 3; (b) d=0.5 μm, corresponding to Fig. 4; and (c) d=1 μm, corresponding to Fig. 5.

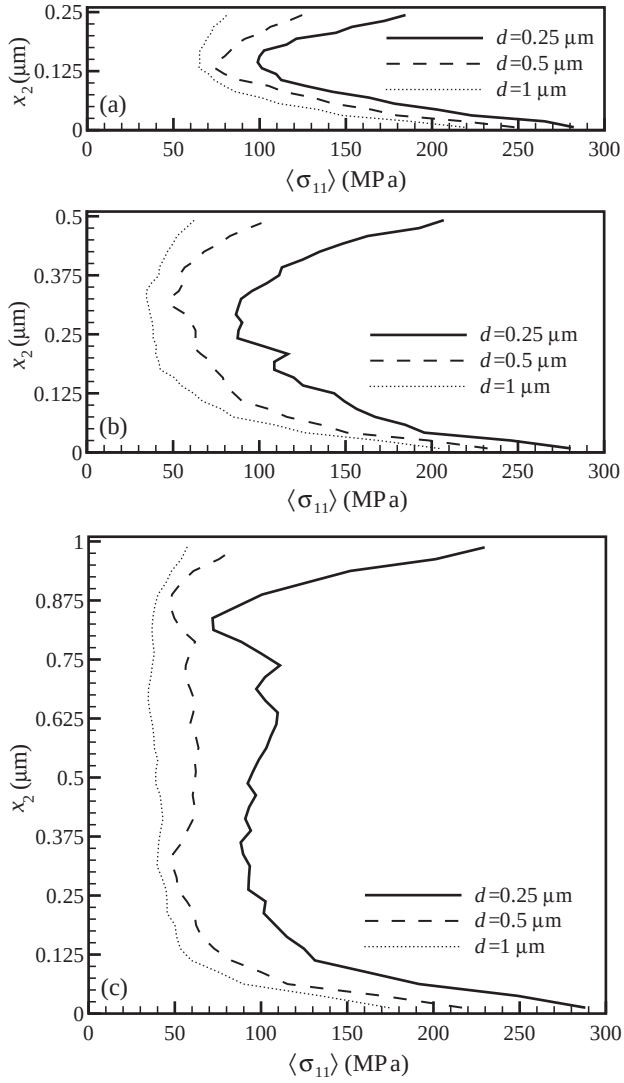

Fig. 7. Variation of average stress, $\langle\sigma_{11}\rangle$, across the film thickness for films of varying grain size and thickness: (a) h=0.25 μm; (b) h=0.5 μm; and (c) h=1 μm. Same data as in Fig. 6 but ordered by grain size.

region (ii) as the surface boundary layer, and region (iii) as the bulk. Boundary layers are also seen in the thicker films (Fig. 6(b) and (c)). In the calculations here, the interface and surface boundary layers have a thickness of about 0.15 μm. In the thickest films, the surface and interface boundary layers are separated by a distinct bulk region, but the size of this region reduces with film thickness. The bulk region is essentially absent in the h=0.25 μm films, for all grain sizes considered.

The average stress in the interface boundary layer is considerably higher than in the rest of the film for any thickness and grain size, see Fig. 6. The highest value of $\langle\sigma_{11}\rangle$ is found in all films at the film–substrate interface. The value of $\langle\sigma_{11}\rangle$ decreases steeply away from the interface to the stress level in the bulk. The magnitude of the stress at the free surface, $\langle\sigma_{11}\rangle(h)$, and the average value in the surface boundary layer increase with decreasing grain size.

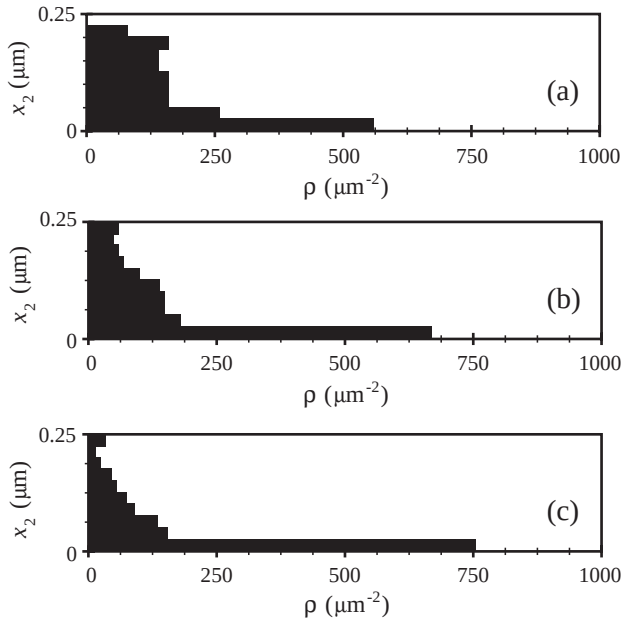

Fig. 8. Dislocation density across the film thickness for films with thickness h=0.25 μm and with various grain sizes: (a) d=0.25 μm; (b) d=0.5 μm; and (c) d=1 μm.

For the films with d=0.25 μm, Fig. 6(a), the average stress in the surface boundary layer is comparable to that in the interface boundary layer, while in the films with d=1 μm the stress at the free surface is only slightly larger than in the bulk (Fig. 6(c)). Moreover, for a given grain size, the magnitude of $\langle\sigma_{11}\rangle$ in the two boundary layers is almost independent of film thickness.

The development of the surface boundary layer is a consequence of the films being polycrystalline. Fig. 6(c) shows the distribution of $\langle\sigma_{11}\rangle$ for films with d=1 μm, which are the closest to a single crystal film: the stress gradient in the surface boundary layer is small. In the results for single crystal thin films of varying thickness presented in [10], a surface boundary layer is not present. On the other hand, an interface boundary layer is present for all single crystal films in [10].

4.2. Grain size dependent response

The data set in Fig. 7 is the same data as in Fig. 6 but with each plot showing the variation of $\langle\sigma_{11}\rangle$ as the grain size varies. The stress in all three regions increases with decreasing grain size. As can be seen by comparing Fig. 7 with the distribution of dislocation density shown in Figs. 8–10 for films with h=0.25, h=0.5 and h=1 μm, respectively, there is a correlation between the density and distribution of dislocations in a film and its stress state. However, the correlation is not simple. The dislocation density close to the film–substrate interface is high in all films and this is where the value of $\langle\sigma_{11}\rangle$ is highest. Yet, the stress magnitude is still lower than the stress that would be present without dislocation activity.

Figs. 8–10 show that the dislocation density close to the interface decreases with decreasing grain size and is roughly independent of the film thickness. In films with narrow grains, dislocations have a higher probability of being stopped by a grain boundary on their way to the interface. Fewer dislocations reach the interface and the region close to it, and therefore the stress in the interface boundary layer is higher in films with narrower grains. Consequently, the density of dislocations in the center of films with narrower grains is considerably higher than in films with wider grains, as seen most clearly in Fig. 10 for 1-μm-thick films.

That many dislocations are stopped by the grain boundaries implies that relatively few dislocations exit the free surface. The highly stressed surface boundary layer appearing in films with a small grain size is a result of this. Stress relaxation depends on the ability of dislocations to glide relatively long distances. Grain boundaries reduce the effective glide distance. Furthermore, the dislocations that glide toward the free surface and that, in a single crystal, would exit at the free surface can be blocked near the free surface by the grain boundaries. This gives rise to the free

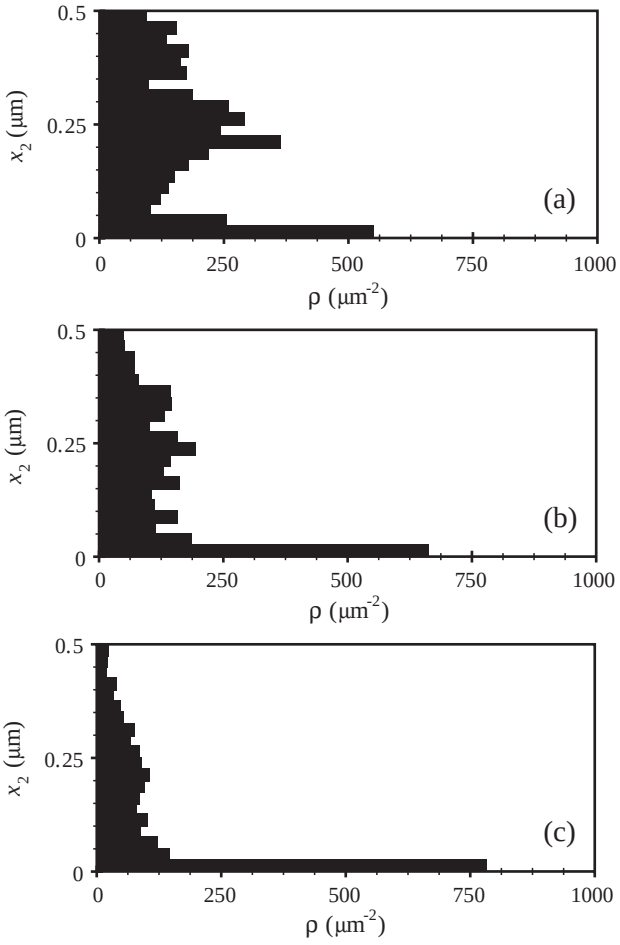

Fig. 9. Dislocation density across the film thickness for films with thickness h=0.5 μm and with various grain sizes: (a) d=0.25 μm; (b) d=0.5 μm; and (c) d=1 μm.

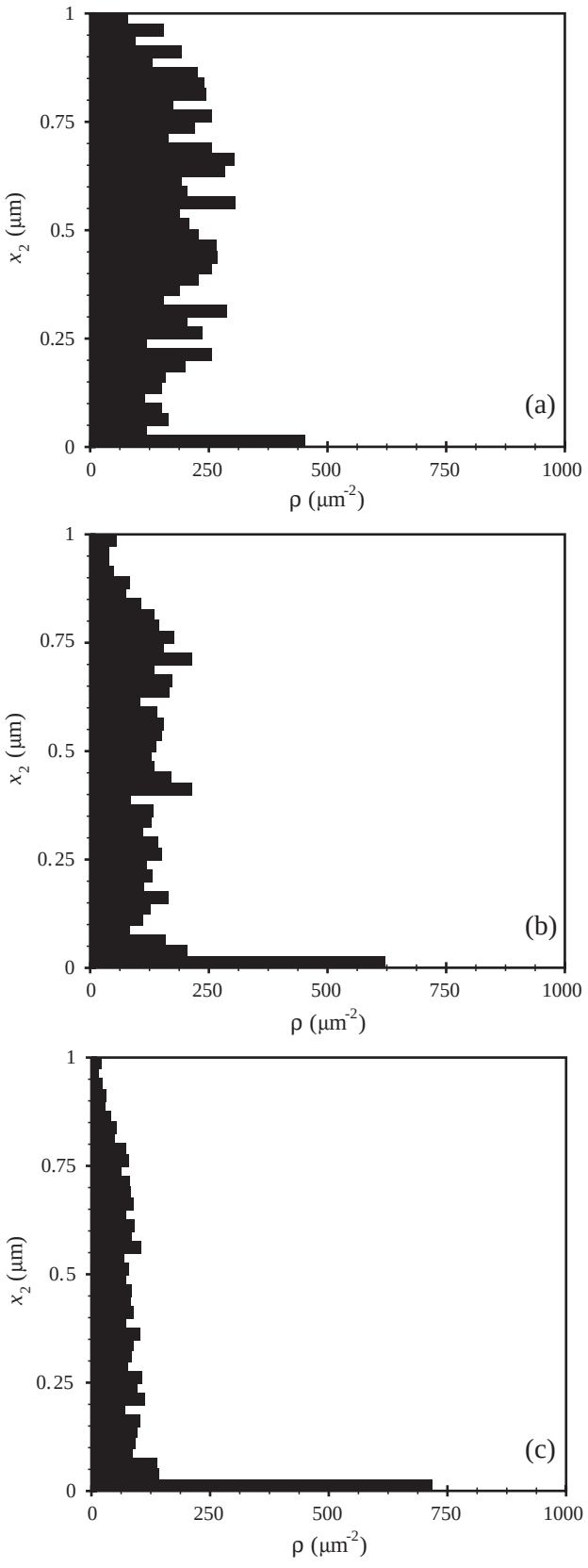

Fig. 10. Dislocation density across the film thickness for films with thickness h=1 μm and with various grain sizes: (a) d=0.25 μm; (b) d=0.5 μm; and (c) d=1 μm.

surface boundary layer in a polycrystal, with more dislocations being blocked in polycrystalline films with small grain size. However, since some of the dislocations do exit at the free surface, the stress level in that boundary layer is less than in the interface boundary layer. The preponderance of slip occurs in the bulk, which acts to reduce the elastic (lattice) strains there and thus lower stress levels in the bulk.

5. Discussion

The results presented in the previous section reveal that polycrystalline films harden with a hardening rate that is dependent on the film thickness as well as on the grain size. Fig. 11 plots the h and d dependence in a manner similar to that in experimental studies, e.g. [4,13,14]. Our results do not obey a simple scaling of power-law type. In Fig. 11(a), the results for d=0.5 μm would fit $\langle\sigma_{11}\rangle_f=\sigma_0+kh^{-1}$ rather well but for thicker grains the scaling approaches Hall–Petch type behavior with an exponent between −1/2 and −1. For narrower grains, however, the scaling exponent tends to be smaller than −1. Actual values for the exponent p are listed in Table 1. The experimental results presented by Venkatraman and Bravman [4] for Al films on Si as well as the results obtained by Dehm et al. [13] on epitaxial Al films on Al_2O_3 predict an inverse relation between stress and film thickness. The study of Baker et al. [15] on textured passivated Cu films shows a similar linear trend for films with ⟨100⟩ texture, while films with ⟨111⟩ texture tend to have a Hall–Petch exponent <−1.

Table 1 also gives values of the exponent q in a grain size scaling law of the type $\langle\sigma_{11}\rangle_f=\sigma_0+k_d d^{-q}$, obtained from the data in Fig. 11(b). The values for the two thicker films are consistent with experimental results of [4], where Hall–Petch exponents for grain size strengthening were found which range from −1 to −1/2.

The coupling between the grain size and film-thickness size dependence is complex. A scaling law of the type

$$\langle\sigma_{11}\rangle_f = \sigma_0 + k_d d^{-q} + k_h h^{-p},$$

as proposed by Venkatraman and Bravman [4] does not provide a good fit to our results; neither did a product expression of the form $\sigma_0(1+k_d d^{-q})(1+k_h h^{-p})$.

The results in Fig. 11 show that the hardening of the polycrystalline films is more affected by reducing the grain size than by reducing the film thickness. The grain size effect would be less pronounced if the grain boundaries were penetrable or partially penetrable to dislocations. In the case of partially penetrable grain boundaries, the dependence of the response on grain orientation would be reduced and the length of the dislocation pile-ups would depend on the grain boundary permeability. In the limit of perfect penetrability, the material will respond as a single crystal. In a similar vein, a partially penetrable film–substrate interface

would give rise to a less pronounced thickness dependent response.

6. Concluding remarks

We have presented two-dimensional discrete dislocation plasticity simulations of stress evolution in polycrystalline films due to a mismatch in thermal expansion coefficient between the film and its substrate. The grains are columnar and have three slip systems with random orientations. Stress relaxation occurs by the nucleation and subsequent glide of edge dislocations. The grain boundaries and the interface with the stiff substrate are treated as impenetrable for the dislocations.

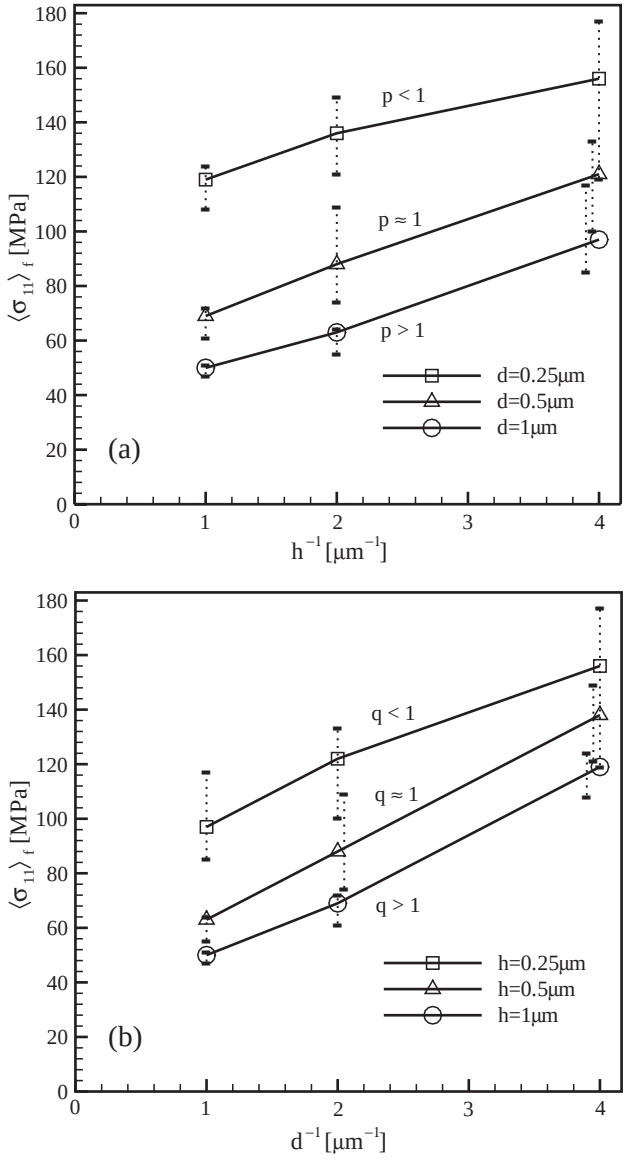

Fig. 11. Average film stress at T=400 K versus (a) film thickness and (b) grain size; p is the exponent in scaling laws of the type $\langle\sigma_{11}\rangle_f=\sigma_0+k_h h^{-p}$, which can be used as a fit to the numerical results in (a). Similarly, q (in b) is the exponent in $\langle\sigma_{11}\rangle_f=\sigma_0+k_d d^{-q}$. Values of all coefficients are given in Table 1.

Table 1
Values of the coefficients in $\langle\sigma_{11}\rangle_f=\sigma_0+k_h h^{-p}$ and $\langle\sigma_{11}\rangle_f=\sigma_0+k_d d^{-q}$ fitted from Fig. 11(a) and (b), respectively

h(μm)	σ_0(MPa)	p	k_h (MPa μm^{-p})
0.25	42	1.4	8
0.5	50	1	19
1	69	0.4	50
d(μm)	σ_0(MPa)	q	k_d (MPa μm−p)
0.25	38	1.4	12
0.5	38	1	25
1	45	0.55	52

The stress that builds up in films after a given temperature change is found to depend on grain size and on film thickness, both in the range of 0.25–1 μm. These size effects are intimately tied to the development of three characteristic regions during deformation:

- an interface boundary layer, independent of film thickness, ≈0.15 μm thick for the parameters used in the calculations, where the average stress is much higher than the bulk average stress; the average stress in this boundary layer increases with decreasing grain size and this increase occurs even without dislocation pile-ups at the interface;
- a surface boundary layer, also approximately 0.15 μm thick, which is a consequence of the films being polycrystalline and which is characterized by an average stress that increases with decreasing grain size; and
- a bulk region between the two boundary layers, where the average stress is lower than the average stress in the film.

While the size of the two boundary layers is essentially independent of film thickness and grain size, their average stress depends on grain size. Thus, the size effect in polycrystalline thin films is a combination of two effects: a thickness-dependent hardening resulting from boundary layers that do not scale with the film thickness and a grain size dependent hardening resulting from an increasing stress level throughout the film with decreasing grain size. The origin of the grain size dependent hardening, i.e. the Hall–Petch effect, is found in the hindering of dislocation motion by grain boundaries coupled with the difficulty of dislocation nucleation in a constrained geometry.

Acknowledgements

This research was carried out under project number MS97007 in the framework of the Strategic Research program of the Netherlands Institute for Metals Research in the Netherlands (www.nimr.nl). AN is grateful for

support from the Materials Research Science and Engineering Center on *On Micro-and-Nano-Mechanics of Electronic and Structural Materials* at Brown University (NSF Grant DMR -0079964).

References

[1] N.A. Fleck, G.M. Muller, M.F. Ashby, J.W. Hutchinson, Acta Metall. Mater. 42 (1994) 475.
[2] J.S. Stölken, A.G. Evans, Acta Mater. 46 (1998) 5109.
[3] H. Huang, J.S. Spaepen, Acta Mater. 48 (2000) 3261.
[4] R. Venkatraman, J.C. Bravman, J. Mater. Res. 7 (1992) 2040.
[5] O. Kraft, L.B. Freund, R. Phillips, E. Arzt, MRS Bull. 27 (2002 January) 30.
[6] W.W. Mullins, Acta Metall. 6 (1958) 414.
[7] Y. Xiang, J.J. Vlassak, M.T. Perez-Prado, Boston, U.S.A., December 1–5, 2003, Materials Research Society Symposium Proceedings, vol. 795, 2004, paper U11.37.1.
[8] E. Van der Giessen, A. Needleman, Model. Simul. Mater. Sci. Eng. 3 (1995) 689.
[9] M.D. Thouless, J. Gupta, J.M.E. Harper, J. Mater. Res. 8 (1993) 1845.
[10] L. Nicola, E. Van der Giessen, A. Needleman, J. Appl. Phys. 93 (2003) 5920.
[11] G. Dehm, D. Weiss, E. Arzt, Mater. Sci. Eng., A Struct. Mater.: Prop. Microstruct. Process. 309–310 (2001) 468.
[12] M.A. Phillips, R. Spolenak, N. Tamura, W.L. Brown, A.A. MacDowell, R.S. Celestre, H.A. Padmore, B.W. Batterman, E. Arzt, J.R. Patel, Microelectron. Eng. 75 (2004) 117.
[13] G. Dehm, T. Wagner, T.J. Balk, E. Arzt, B.J. Inkson, J. Mater. Sci. Technol. 18 (2002) 113.
[14] O.S. Leung, A. Munkholm, S. Brennan, W.D. Nix, J. Appl. Phys. 88 (2000) 1389.
[15] S.P. Baker, A. Kretschmann, E. Arzt, Acta Mater. 49 (2001) 2145.